


Available online at www.sciencedirect.com
ScienceDirect
Procedia IUTAM 16 (2015) 50 – 59
Procedia IUTAM
www.elsevier.com/locate/procedia

IUTAM Symposium on Dynamics of Capsules, Vesicles and Cells in Flow

Migration of elastic capsules by an optical force in a uniform flow

Cheong Bong Chang[a], Wei-Xi Huang[b,*], Hyung Jin Sung[a,*]

[a]*Department of Mechanical Engineering, KAIST, Daejeon 305-701, Korea*
[b]*Department of Engineering Mechanics, Tsinghua University, Beijing 10084, China*

Abstract

The behavior of an elastic capsule by an optical force in a uniform flow is examined by using the penalty immersed boundary method. The elastic capsule is subjected to the laser beam with Gaussian distribution in the perpendicular direction to the fluid flow. The elastic capsule migrated by the optical force along the direction of the laser beam propagation, and the migration distance is dependent on its properties. The oblate capsule with $b/a = 0.5$ obeying the neo-Hookean constitutive law is first considered, and the effects of the surface Young's modulus and the initial inclination angle on the migration distance are studied. The migration distance of the oblate capsule is increased as the surface Young's modulus increases, and the non-inclined oblate capsule is more migrated than the differently inclined capsules. Then the spherical, oblate, and biconcave capsules obeying the Skalak constitutive law are considered. A comparison of the trajectories of the capsules indicates that the migration of the spherical capsule is the largest. Unlike the oblate capsule, the non-inclined biconcave capsule is less migrated than other inclination angles due to its initial shape.

Peer-review under the responsibility of the organizing committee of DYNACAPS 2014 (Dynamics of Capsules, Vesicles and Cells in Flow).

Keywords: Elastic capsule; Optical force; Dynamic ray tracing method; Penalty immersed boundary method

1. Introduction

Blood cells consist of red blood cell (RBC), white blood cell, and platelet, which have different shapes and properties. Among them, RBC is made of cytoplasm and cell membrane without a nucleus. Due to its simple

* Corresponding author. Tel.: +82-42-350-3027; +86-10-6279-7215
E-mail address: hjsung@kaist.ac.kr; hwx@tsinghua.edu.cn

Peer-review under the responsibility of the organizing committee of DYNACAPS 2014 (Dynamics of Capsules, Vesicles and Cells in Flow).
doi:10.1016/j.piutam.2015.03.007

structure, the dynamics of RBC assumed as an elastic capsule has been widely studied under various external forces such as hydrodynamic force, magnetic force, optical force, and acoustic force.[1, 2] In the simple shear flow, a biconcave capsule to mimic the RBC exhibited the swinging and tumbling motions depending on the capillary number and the reduced bending modulus.[3, 4] The lateral migration distance of the spherical elastic capsule by the optical force in a uniform flow is varied with the elastic properties.[5] The RBC is softened or stiffened by disease,[6] so understanding the behavior of the elastic capsule with different elastic properties and shapes under an external force is important for separation of abnormal blood cells from normal ones.

The optical force has been widely used to manipulate and separate particles or cells because it is controllable in the pico-Newton scale on an object of micro-scale size in a noncontact manner.[7] Under a loosely focused laser beam with Gaussian distribution, the optical force pushes the object along the direction of the laser beam propagation, while horizontally pulls the object to the laser beam axis. The axial motion along the direction of the laser beam propagation can be restricted by using a tightly focused laser beam, which was used to manipulate a single particle or cell. For separation of multiple particles or cells, the fluid flow was imposed in the optical method. In the optical chromatography, a single loosely focused laser beam oppositely directed to the fluid flow was adopted.[8, 9] The particles or cells moved with the fluid flow stop at the equilibrium position between the optical force and the viscous force. The optical force depends on the properties of the particle or cell such as the size, shape, refractive index and elastic properties. Hence, the particle or cell with different properties can be separated. In the cross-type optical separation (COPS),[10-12] a single loosely focused laser beam is also used, but the direction of the laser beam propagation is perpendicular to the fluid flow. The particles or cells moving by the fluid flow pass through the illuminated region by the laser beam, and migrates in this region along the direction of the laser beam propagation. After escaping from the illuminated region, they again move with the fluid flow, retaining the lateral migration distance. Hence, the continuous separation of particles or cells is available in the COPS.

The separation of spherical rigid particles with different properties in the COPS was studied numerically and experimentally.[10-12] For simulation, the particle motion equation including the optical force term is solved. The optical force is calculated by the ray optics method, which is applicable for the object size larger than the wavelength of the laser beam.[5, 10, 13-16] Spherical particles can be separated according to the size and the ratio of the refractive indices. An oblate particle was also considered in the COPS.[17] Due to the shape, the optical force on the oblate particle was obtained by the dynamic ray tracing method using the ray-triangle intersection algorithm.[18] The optical force term was included in the particle motion equation, and the penalty immersed boundary method (pIBM) developed by Huang *et al.*[19] was used for the fluid-particle interaction. In a stationary fluid, the oblate particle rotates near the laser beam axis by the optically induced torque until the major semi-axis of the particle is aligned with the laser beam axis.[20] During the rotation, the oblate particle is horizontally pulled or repelled according to the orientation of the major semi-axis. Such a horizontal optical force affects the migration distance in the COPS. Considering the oblate particle already aligned with the laser beam axis, the particle does not rotate during the whole movement. Hence, the migration distance of the oblate particle is increased as the aspect ratio increases. On the other hand, the migration distance is varied with the initial inclination angle due to the horizontal optical force induced by the rotation. When the direction of the horizontal optical force induced by the rotation is matched with the direction of the fluid flow, the effect of the inclination angle is enhanced. Hence, the rotation about the spanwise direction has to be suppressed for effective separation of oblate particles according to the aspect ratio.

The migration of a spherical elastic capsule by the optical force in a uniform flow was also examined.[5] During the migration of the capsule by the optical force, the capsule membrane is deformed by the optical force, and the deformed shape affects the lateral migration. To simulate the deformation of the capsule, the membrane motion equation is solved, and the pIBM was adopted for the fluid-membrane interaction. The results for different elastic properties, i.e. the surface Young's modulus and the bending modulus, showed that the migration distance mainly depends on the surface Young's modulus. The migration distance of the capsule is increased as the surface Young's modulus increases. Although the bending modulus does not affect much the migration distance, the buckling occurring on the capsule with high surface Young's modulus is suppressed by increasing the bending modulus. To the best of our knowledge, study on the non-spherical elastic capsule in the COPS has not been carried out so far, although the RBC among the blood cells is not spherical and deformable. For the elastic capsule, the optical force and the deformed shape are interacted with each other, and the deformed shape also affects the rotation. Hence, the

oblate and biconcave capsule may show different behaviors in the COPS, comparing with the spherical capsule and the oblate particle.

In the present study, the migration of elastic capsules subjected to the optical force in a uniform flow is simulated. The effects of the elastic properties and the shapes on the migration distance are examined. To solve such system, the pIBM is adopted for solving the fluid-membrane interaction, and the dynamic ray tracing method is used to calculate the optical force. The obtained optical force is included in the membrane motion equation. First, the oblate capsule with b/a = 0.5 obeying the neo-Hookean (NH) constitutive law is simulated. Variations of the migration distance with the surface Young's modulus and the initial inclination angle are examined. Next, the biconcave capsule obeying the Skalak (SK) constitutive law is considered to mimic the RBC. For comparison, the spherical and oblate capsules assumed as the SK membrane are also simulated, and variations of the migration distance with the initial inclination angle are presented.

2. Problem formulation and numerical method

2.1. Fluid-membrane interaction

The optically induced migration of an elastic capsule in a uniform flow is studied as shown in Fig. 1. The capsule is assumed to be enclosed by a membrane without thickness, and the fluid-membrane interaction is implemented by the pIBM. In the framework of the pIBM, the governing equations for the fluid flow and the membrane motion are separately solved in different coordinates, and are coupled by an additional momentum forcing to enforce the no-slip condition on the solid boundary.

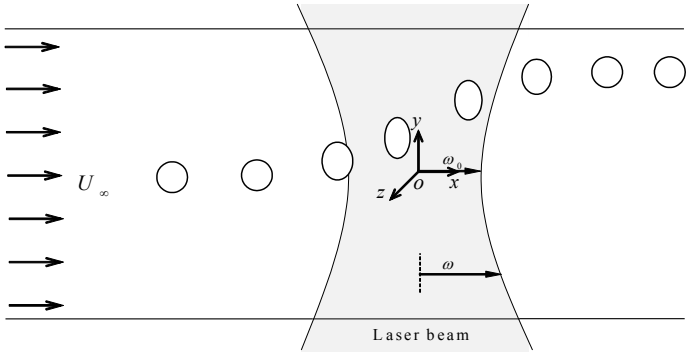

Fig. 1. Schematic diagram of the elastic capsule subjected to the laser beam in a uniform flow.

The fluid flow is governed by the Navier-Stokes and continuity equations in the Eulerian coordinates, which are expressed by

$$\rho_0 \left(\frac{\partial \boldsymbol{u}}{\partial t} + \boldsymbol{u} \cdot \nabla \boldsymbol{u} \right) = -\nabla p + \mu \nabla^2 \boldsymbol{u} + \boldsymbol{f}, \tag{1}$$

$$\nabla \cdot \boldsymbol{u} = 0, \tag{2}$$

where ρ_0, $\boldsymbol{u}$, p, μ, and f are the fluid density, the fluid velocity, pressure, viscosity, and Eulerian momentum forcing, respectively. The equation of the membrane motion defined in the moving Lagrangian coordinate system is expressed by

$$\rho \frac{\partial^2 \boldsymbol{X}}{\partial t^2} = \sum_{i,j=1}^{2} \left[\frac{\partial}{\partial s_i} \left(S_{ij} \frac{\partial \boldsymbol{X}}{\partial s_j} \right) - \frac{\partial}{\partial s_i \partial s_j} \left(B_{ij} \frac{\partial^2 \boldsymbol{X}}{\partial s_i \partial s_j} \right) \right] - \boldsymbol{F} + \boldsymbol{F_o}, \tag{3}$$

where ρ , $\boldsymbol{X}$, S_{ij}, B_{ij}, $\boldsymbol{F}$, and $\boldsymbol{F}_o$ are the density difference between the solid and fluid, the position of the membrane, the second Piola-Kirchhoff stress tensor, the bending stress tensor, Lagrangian momentum forcing, and the optical force, respectively. (s_1, s_2) denotes the moving curvilinear coordinates. S_{ij} and B_{ij} are derived by using the energy method.[4] S_{ij} for the NH and SK constitutive laws is expressed as,

$$S_{ij}^{\mathrm{NH}} = \frac{E_S}{3} \left[\delta_{ij} - \frac{(-1)^{i+j}}{(I_2+1)^2} \left(\delta_{ij} + 2D_{3-i,3-j} \right) \right], \quad (i,j=1,2), \tag{4}$$

$$S_{ij}^{\mathrm{SK}} = \frac{E_S}{2} \left[(I_1+1)\delta_{ij} + (-1)^{i+j} (CI_2 - 1) \left(\delta_{ij} + 2D_{3-i,3-j} \right) \right], \quad (i,j=1,2), \tag{5}$$

where E_s and D_{ij} are the surface Young's modulus and the Green strain tensor, and C is a constant related to the area dilation. B_{ij} is expressed by using the bending strain tensor K_{ij} as follows,

$$B_{ij} = \gamma \left[(K_{11} + K_{22})\delta_{ij} - (-1)^{i+j} (1-\nu_s) K_{3-i,3-j} \right] \Big/ \left| \frac{\partial^2 \boldsymbol{X}}{\partial s_i \partial s_j} \right|, \quad (i,j=1,2), \tag{6}$$

where γ and ν_s are the bending coefficient and Poisson ratio, respectively. In the present study, ν_s is simply set to zero.[4]

In the pIBM, to couple the fluid flow and the solid motion, two kinds of the immersed boundaries are assumed, i.e. the massless and massive material points. Motions of the massless material points are computed from the interpolation of the Eulerian fluid velocity by using the smoothed Dirac delta function,[21] while the motion of the massive material points are directly obtained by solving the equation of the solid motion. The two kinds of the immersed boundaries are linked closely by a stiff spring with damping, so they are moved together like a single massive structure. The restoring force on the Lagrangian immersed boundary is calculated by

$$\boldsymbol{F}(s_1, s_2, t) = -\kappa \left[(\boldsymbol{X}_{ib} - \boldsymbol{X}) + \Delta t (\boldsymbol{U}_{ib} - \boldsymbol{U}) \right], \tag{7}$$

where κ and Δt denote a large coefficient and the computational time step, respectively. $\boldsymbol{X}$ and $\boldsymbol{X}_{ib}$ denote the positions of the massive and massless material points, and the $\boldsymbol{U}$ and $\boldsymbol{U}_{ib}$ are the corresponding velocities. The Lagrangian momentum forcing is spread on the Eulerian grids as follows,

$$\boldsymbol{f}(\boldsymbol{x}, t) = \int_{\Omega_S} \boldsymbol{F}(s_1, s_2, t) \delta \left(\boldsymbol{x} - \boldsymbol{X}(s_1, s_2, t) \right) \mathrm{d}s_1 \mathrm{d}s_2, \tag{8}$$

where $\delta(\,)$ is the smoothed Dirac delta function. Here, the four-point smoothed delta function is used in simulation.[21]

For computation, the governing equations are non-dimensionalized by using the characteristic scales. The fluid density ρ_0 , the far-field velocity U_∞ , and the minimum waist radius of the laser beam ω_0 are selected as the characteristic density, velocity, and length, respectively. After the non-dimensionalization, the governing equation takes the same forms, except that ρ_0 is removed and μ is replaced by $1/Re$ in Eq. (1). The membrane is discretized by using the subdivision surface method.[22] The governing equations for the fluid flow and the membrane motion are solved by the fractional step method[23] and the subdivision finite element method,[4] respectively. They are coupled by the pIBM.[19] More details of the numerical method can be found in Hunag *et al.*.[4, 19]

2.2. Calculation of the optical force

The ray optics method is adopted for calculation of the optical force. In the ray optics method, the light from the laser beam is assumed as a bundle of rays with direction and momentum. Due to the difference in the refractive indices, some of the momentum with a ray is reflected and the rest is refracted. At the same time, the direction is also changed. The momentum change per unit time is defined as the optical force, which on each nodal point is expressed as

$$\boldsymbol{F}_{o,i} = \frac{n_m}{c}\frac{P_{g,i}}{\Delta A_i}\boldsymbol{Q}_i, \tag{9}$$

where i, n_m, c, $\boldsymbol{Q}$ denote the index of surface elements, the refractive index of the outer fluid, the speed of the light, and the dimensionless momentum transfer, respectively. P_g is the incident laser beam power, which is defined as $P_{g,i} = (\boldsymbol{I}_i \cdot \boldsymbol{N}_{e,i})\Delta A_i$, where ΔA, N_e, and $\boldsymbol{I}$ are the area around nodal point, the surface normal direction of the element, and the Gaussian beam intensity, respectively. In the present study, a loosely focused laser beam with the Gaussian distribution is used, so the beam intensity has only a y- component, as expressed as

$$I = \frac{2P}{\pi\omega(y)^2}\exp\left[-\frac{2d_f^2}{\omega(y)^2}\right], \tag{10}$$

where P and d_f are the laser beam power and the distance from the focal point to each nodal point, and ω is the waist radius of the laser beam.

The dimensionless momentum transfer indicates the direction of the optical force, and is calculated using the direction vectors of the incident, refracted, and reflected rays, i.e. $\boldsymbol{Q}$ = (incident ray) – (reflected ray) – (refracted ray). The ray-triangle intersection algorithm is used for the dynamic ray tracing because the elastic capsule subjected to the laser beam is deformed.[18] The incident ray from the laser beam firstly intersects the lower surface of the capsule, and then the refracted ray on the lower surface intersects the upper surface of the capsule. In the present study, the ratio of the refractive indices is not large, so only the refracted ray is traced.[5, 13, 16] During the tracing of the refracted ray, P_g calculated at the first intersection element is consistently used. Details of the computational procedure can be found in the previous studies.[5, 16] In the following paragraphs, the non-dimensional quantities are used by default, while the star superscript is marked on the dimensional ones to avoid confusion.

3. Results and discussion

The lateral migration of the elastic capsule by the optical force in a uniform is simulated. The equivalent radius defined by $r_{eq}^* = \sqrt{A^*/\pi}$ is set to be 3.2μm for both the oblate capsule with b/a = 0.5 and the biconcave capsule, where A denotes the surface area of the capsule membrane, and it is non-dimensionalized by the minimum waist radius of the laser beam. The capsule is moved by the fluid flow with n_m = 1.33 and Re = 0.01 based on U_∞^* = 625μm/s and ρ_0^* = 1000kg/m^3, and is subjected to the Gaussian laser beam with ω_0^* = 16μm, λ^* = 1.064μm, and P^* = 3.4W. The properties of the inner fluid of the capsule are the same as those of the outer fluid, except for the refractive index of the inner fluid n_p = 1.40. The capsule membrane is discretized using 8192 triangular elements. The elastic properties of the membrane is set similarly with those of the RBC.[24, 25] The surface Young's modulus and the bending rigidity are varied in the ranges of E_s^* = 0.625 - 2.5×10^{-5} N/m and γ^* = 3.2 - 4.0×10^{-19} Nm, respectively. To present the variation of the elastic properties, the capillary number and the reduced bending modulus are used, which are defined as $\mathrm{Ca} = \mu U_\infty / E_s$, and $\zeta = \gamma / r_{eq}^2 E_s$. The density difference of ρ = 0.1 is set in the simulations.

The fluid domain has a size of $36r_{eq}$×$76r_{eq}$×$18r_{eq}$, and is discretized using 256×320×128 grids in the x-, y-, and z-directions. The uniform grids are distributed in the x- and z- directions, but the stretched grid is generated in the y-direction except for a $36r_{eq}$ width near the center of the domain. The origin of the coordinates is located at the center of the domain in the x- and z- directions, and at a distance of $28r_{eq}$ from the bottom of the domain in the y- direction.

For a uniform flow, $u = U_\infty$, $v = w = 0$ is enforced at the inlet, top, and bottom of the domain. The convective boundary condition is adopted at the outlet of the domain, and the periodic boundary condition is applied in the z-direction. The laser beam axis is along the z- axis, and the capsule is initially released at $x = -15r_{eq}$, $y = 0$, and $z = 0$. In the simulations, the computational time step $\Delta t = 0.00001$ is used, and the free constant $\kappa = 2.8 \times 10^8$ is set, which is large enough to assure the convergence of the solution.

3.1. The oblate capsule with b/a = 0.5 in the COPS

The oblate capsule with $b/a = 0.5$ obeying the NH constitutive law is first considered, and the effects of the elastic properties and the inclination angle on the migration distance are examined. The inclination angle θ is defined as the angle between the major semi-axis of the capsule and the positive x- axis in the x-y plane with $z = 0$, because the effect of the inclination is maximized when the capsule rotated about the z- axis (spanwise direction).[17] The major semi-axis of the non-inclined oblate capsule is parallel with the x-z plane. Since the migration distance of the elastic capsule is mainly dependent on the surface Young's modulus,[5] the bending coefficient is fixed in the present study. As the surface Young's modulus increases, both the capillary number and the reduced bending modulus decrease.

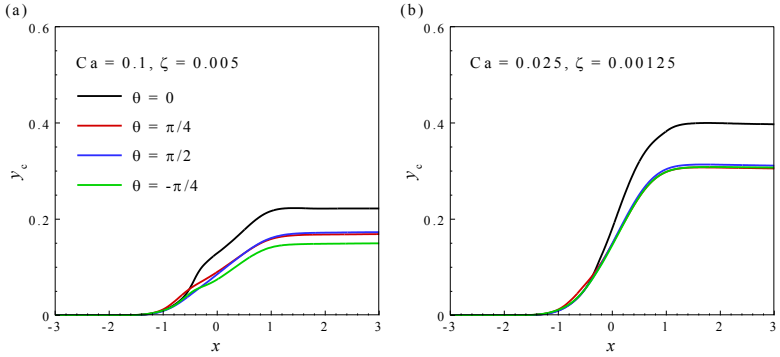

Fig. 2. Trajectories of the differently inclined oblate capsule with $b/a = 0.5$: (a) Ca = 0.1 and $\zeta = 0.005$; (b) Ca = 0.025 and $\zeta = 0.00125$.

The trajectories of the oblate capsule with different Ca and ζ are shown in Fig. 2. Generally, the oblate capsule moved by the fluid flow is laterally migrated near the laser beam axis. After escaping from the illuminated region of the laser beam, the capsule again is moved following the fluid flow, retaining the lateral migration distance. The migration distance for each inclination angle is increased with the decrease of Ca and ζ, indicating that the more deformable capsule is less migrated by the optical force. For different initial inclination angles, it is shown that the initially inclined oblate capsules are similarly migrated, while the non-inclined case achieves a larger lateral migration distance. Such effect of the inclination angle is different with that on the particle case, where the migration distance of the positively (negatively) inclined oblate particle is increased (decreased) because the particle is decelerated (accelerated) by the horizontal optical force.[17]

The variation of the migration distance by the initial inclination angle is caused by the deformation and the rotation of the capsule, which is shown by the instantaneous shape of the oblate capsule and the distribution of the optical force in Fig. 3. The optical force is along the surface normal direction and is calculated by

$$F_{o,i} = \sqrt{F_{o,x,i}^2 + F_{o,y,i}^2 + F_{o,z,i}^2}\,\Delta A_i, \tag{11}$$

which is non-dimensionalized by $\rho_0 U_\infty^2 \omega_0^2$. As shown in Fig. 3(c) and 3(d), the capsule is stretched along the direction of the laser beam propagation when approaching the laser beam axis. Hence, the major semi-axis of the

oblate capsule is rapidly aligned to the laser beam axis, and the horizontally acted optical force on the upper surface is diminished. Then the oblate capsule with $\theta = \pi/4$ and $-\pi/4$ is moved like the $\theta = \pi/2$ case, and they are similarly migrated as seen in Fig. 2. The oblate capsule with $\theta = \pi/2$ is stretched along the major semi-axis, whereas the non-inclined capsule is stretched along the minor semi-axis. Therefore, the extent of deformation becomes different, and the capsules are differently migrated.

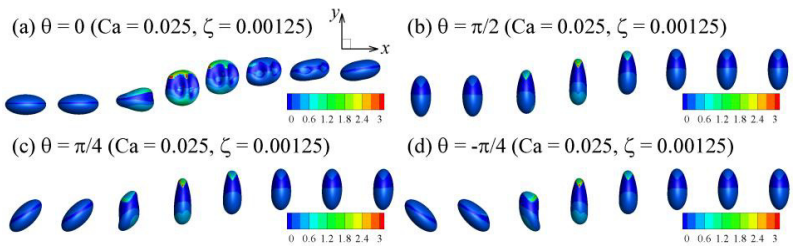

Fig. 3. Instantaneous shapes and optical force distributions of the oblate capsule with $b/a = 0.5$: (a) $\theta = 0$; (b) $\theta = \pi/2$; (c) $\theta = \pi/4$; (d) $\theta = -\pi/4$.

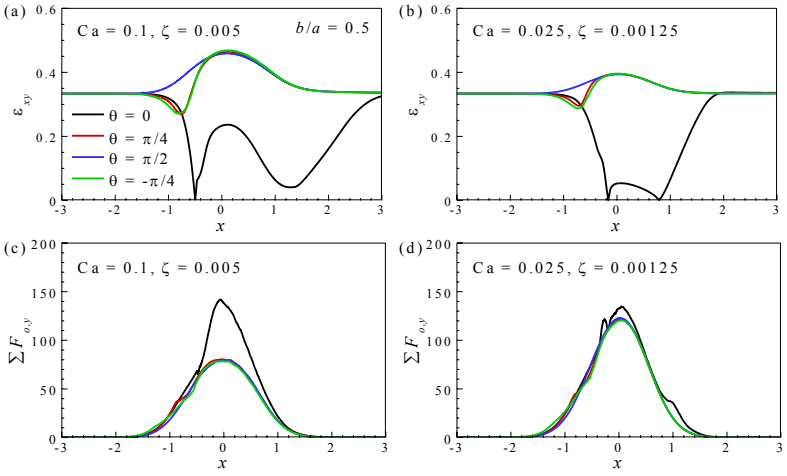

Fig. 4. The deformation parameter of the oblate capsule with (a) Ca = 0.1, $\zeta = 0.005$ and (b) Ca = 0.025, $\zeta = 0.00125$, and the y- component optical force of the oblate capsule with (c) Ca = 0.1, $\zeta = 0.005$ and (d) Ca = 0.025, $\zeta = 0.00125$ as functions of the streamwise position.

To examine the effect of the surface Young's modulus on the capsule motion, variations of the deformation parameter and the y- component optical force with the streamwise position are shown in Fig. 4. The deformation parameter is defined as

$$\varepsilon_{xy} = \frac{|L_1 - L_2|}{L_1 + L_2}, \tag{12}$$

where L_1 and L_2 are the length of the major and minor semi-axes of the capsule on the plane $z = 0$. The y- component optical force is calculated by

$$\sum F_{o,y} = \sum_{i=1}^{NE} F_{o,y,i} \Delta A_i, \tag{13}$$

which is non-dimensionalized by $\rho_0 U_\infty^2 \omega_0^2$. As shown in Fig. 4(a) and 4(b), the deformation parameter is largely varied for the high Ca and ζ. When the extent of deformation is reduced, the *y*- component optical force is increased. As shown in Fig. 4(c) and 4(d), all the *y*- component optical force except for the non-inclined case are similarly varied. Although the *y*- component optical force of the non-inclined capsule of the high Ca and ζ is larger than that of the small Ca and ζ, the optical force of the capsule of the high Ca and ζ is more consumed by deformation. Hence, the oblate capsule with higher surface Young's modulus is more migrated.

In summary, the results for the oblate capsule show that the stiffer capsule can be more migrated in the COPS. The variation of the initial inclination angle affects differently the trajectories of the oblate particle and capsule. The horizontal optical force induced by the inclination of the oblate capsule is diminished due to the capsule deformation. Furthermore, the extent of the deformation becomes different according to the initial inclination angle, which also causes the difference in the migration distance. In the simulation, the NH law is adopted for the capsule membrane, but the membrane of the RBC is typically assumed as the SK material. The RBC is usually modelled as a biconcave capsule, and the NH membrane is more elastic than the SK membrane, so different behaviors may be induced in the COPS. In the next subsection, the elastic capsule with various shapes obeying the SK constitutive law is considered, and effect of the membrane constitutive law is also presented.

3.2. The RBC model in the COPS

The behavior of the biconcave capsule obeying the SK constitutive law to mimic the RBC is examined. For comparison, the spherical capsule and the oblate capsule with b/a = 0.5 obeying the SK constitutive law are also included. In simulations, Ca = 0.03125 and ζ = 0.001953 are fixed. The constant related to the area dilation C is set to be 50, which results in a nearly area-incompressible membrane. The capsule is subjected to the laser beam with P^* = 2.66W. The computational time step Δt = 0.000008 is used. Figure 5 shows the trajectories of the elastic capsule with different shapes. The spherical capsule is more migrated than other capsules, which was also observed for the spherical and oblate particles in the COPS.[17] According to the initial inclination angle, different trends are shown for the oblate and biconcave capsules. As shown in Fig. 5(b), the biconcave capsule with different inclination angles is similarly migrated except for the non-inclined case having a smaller migration distance. On the other hand, all the oblate capsules are similarly migrated, which is different with those obeying the NH constitutive law as discussed above.

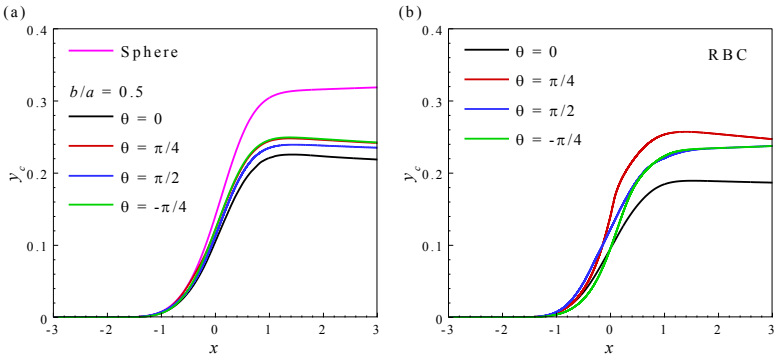

Fig. 5. Trajectories of the differently inclined elastic capsules: (a) spherical and oblate capsules; (b) biconcave capsule.

The behavior of the elastic capsules with different shape is clearly seen from the instantaneous shape and the optical force distribution in Fig. 6. As shown in Fig. 6(a)-(d), the major semi-axis of the oblate capsules except for the non-inclined case was aligned with the laser beam axis, and they are similarly migrated, which is the same as the NH membrane cases. Although the laser beam power in the simulation is reduced, the deformation of the capsule

with SK membrane is reduced mainly due to the strain hardening effect by the restriction of the area dilation. Hence, the initial shape of the non-inclined oblate capsule is almost preserved during the deformation. Since the migration distances of the oblate particle with $\theta = 0$ and $\pi/2$ are similar,[17] the migration distances of the oblate capsule with $\theta = 0$ and $\pi/2$ are also not much different, indicating that the stiff oblate capsule can similarly migrate regardless of the initial inclination angle.

Unlike the oblate case, the dimples of the biconcave capsule affects significantly the migration distance. For the biconcave capsule initially aligned with the laser beam axis, the incident ray from the laser beam intersects with the capsule surface three or four times due to the presence of the dimple, during passing through the capsule. As a result, the biconcave capsule with $\theta = \pi/2$ can be more migrated than the non-inclined case. As shown in Fig. 6(e)-(h), although the initially inclined biconcave capsules except for $\theta = \pi/2$ case are not exactly aligned with the laser beam axis, the capsules are sufficiently rotated near the laser beam axis. Hence, the biconcave capsules can be similarly migrated, except for the non-inclined case having a smaller migration distance.

The above results for the elastic capsules with different shapes show that the spherical shape is beneficial for the lateral migration in the COPS. The effect of the initial inclination angle on the migration distance is different according to the shape of the capsule. Unlike the oblate capsule, the biconcave capsule aligned with the laser beam axis can be more migrated than the non-inclined case. The migration distance of the oblate capsule obeying the NH or SK constitutive law show different trends for different initial inclination angles because the SK membrane is relatively stiffer than the NH membrane.

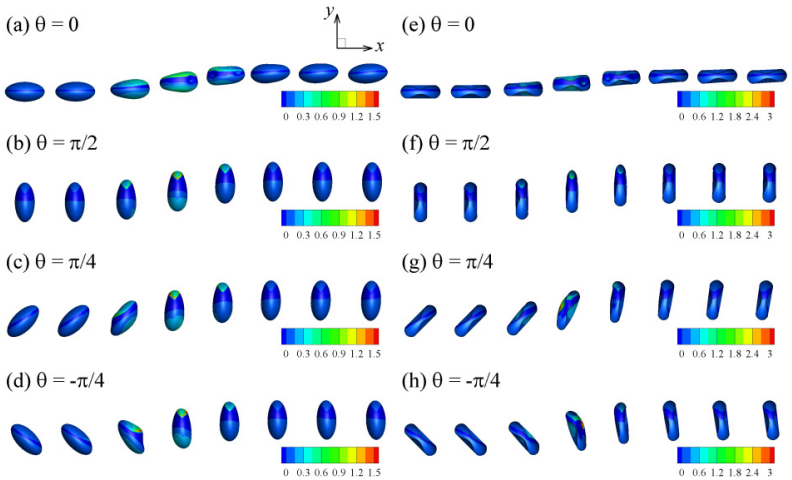

Fig. 6. Instantaneous shapes and optical force distribution of (a)-(d) the oblate capsule with $b/a = 0.5$ and (e)-(h) biconcave capsule.

4. Conclusions

In the present study, the lateral migration of the elastic capsules in the COPS was numerically investigated. To simulate such system, the pIBM for the fluid-membrane interaction was adopted, and the optical force was obtained by the dynamic ray tracing method. First, the oblate capsule with $b/a = 0.5$ obeying the NH constitutive law was considered. The effects of the surface Young's modulus and the initial inclination angle on the migration distance were presented. The results showed that the oblate capsule with higher surface Young's modulus was more migrated. The differently inclined oblate capsule was similarly migrated, except for the initially non-inclined case having a higher migration distance. Next, the behavior of the elastic capsule with different shapes obeying the SK constitutive law was examined. It was shown that the migration of the spherical capsule was the largest. Since the biconcave capsule aligned with the laser beam axis received more momentum from the laser beam than the non-inclined case, the migration distance of the initially non-inclined biconcave capsule was smaller than the differently inclined ones.

Acknowledgments

This work was supported by the Creative Research Initiatives (No. 2014-001493) program of the National Research Foundation of Korea (MSIP). W.-X. Huang acknowledges the support from the NSFC (No. 11322221).

References

1. Pamme N. Continuous flow separations in microfluidic devices. *Lab Chip* 2007;**7**:1644-1659.
2. Chen J, Li J, Sun Y. Microfluidic approaches for cancer cell detection, characterization, and separation. *Lab Chip* 2012;**12**:1753-1768.
3. Le DV. Effect of bending stiffness on the deformation of liquid capsules enclosed by thin shells in shear flow. *Phys Rev E* 2010;**82**;016318.
4. Huang WX, Chang CB, Sung HJ. Three-dimensional simulation of elastic capsules in shear flow by the penalty immersed boundary method. *J Comput Phys* 2012;**231**:3340-3364.
5. Chang CB, Huang WX, Sung HJ. Lateral migration of an elastic capsule by optical force in a uniform flow. *Phys Rev E* 2012;**86**:066306.
6. Lee GYH, Lim CT. Biomechanics approaches to studying human disease. Trends Biotechnol 2007;**25**:111-118.
7. Ashkin A. History of optical trapping and manipulation of small-neutral particle, atoms, and molecules. *IEEE J Sel Top Quantum Elec* 2000;**6**:841-856.
8. Hart SJ, Terray AV. Refractive-index driven separation of colloidal polymer particles using optical chromatography. *Appl Phys Lett* 2003;**83**: 5316-5318.
9. Hebert CG, Terray A, Hart SJ. Toward label-free optical fractionation of blood-optical force measurements of blood cells. Anal Chem 2011;**83**:5666-5672.
10. Kim SB, Kim JH, Kim SS. Theoretical development of in situ optical particle separator: cross-type optical chromatography. *Appl Opt* 2006;**45**: 6919-6924.
11. Kim SB, Yoon SY, Sung HJ, Kim SS. Cross-type optical particle separation in a microchannel. *Anal Chem* 2008;**80**:2628-2630.
12. Kim SB, Lee KH, Sung HJ, Kim SS. Nonlinear particle behavior during cross-type optical particle separation. *Appl Phys Lett* 2009;**95**:264101.
13. Bareil PB, Sheng Y, Chiou A. Local scattering stress distribution on surface of a spherical cell in optical stretcher. *Opt Express* 2006;**14**:12503-12509.
14. Ashkin A. Forces of a single-beam gradient laser trap on a dielectric spheres in the ray optics regime. *Biophys J* 1992;**61**:569-582.
15. Kim SB, Kim SS. Radiation forces on spheres in loosely focused Gaussian beam: ray-optics regime. *J Opt Soc Am B* 2006;**23**:897-903.
16. Sraj I, Szatmary AC, Marr DWM, Eggleton CD. Dynamic ray tracing for modeling optical cell manipulation. *Opt Express* 2010;**18**:16702-16714 .
17. Chang CB, Huang WX, Lee KH, Sung HJ. Optical separation of ellipsoidal particles in a uniform flow. *Phys Fluids* 2014;**26**:062001.
18. Möller T, Trumbore B. Fast, minimum storage ray-triangle intersection. *J Graphics GPU Games Tools* 1997;**2**:21-28.
19. Huang WX, Chang CB, Sung HJ. An Improved Penalty Immersed Boundary Method for Fluid-Flexible Body Interaction. *J Comput Phys* 2011;**230**:5061-5079.
20. Chang CB, Huang WX, Lee KH, Sung HJ. Optical levitation of a non-spherical particle in a loosely focused Gaussian beam. *Opt Express* 2012;**20**:24068-24084.
21. Peskin CS. The immersed boundary method. *Acta Numer* 2002;**11**:479-517.
22. Cirak F, Ortiz M, Schroder P. Subdivision surfaces: a new paradigm for thin-shell finite-element analysis. *Int J Numer Meth Engng* 2000;**47**:2039-2072.
23. Kim K, Baek SJ, Sung HJ. An implicit velocity decoupling procedure for incompressible Navier-Stokes equations. *Int J Numer Meth Fluids* 2002;**38**:125-138.
24. Hochmuth RM. Measuring the mechanical properties of individual human blood cells. *J Biomech.Eng* 1993;**115**:515-519.
25. Evans EA. Bending elastic modulus of red blood cell membrane derived from buckling instability in micropipette aspiration tests. *Biophys J* 1983;**43**:27-30.